Dynamics of a three-terminal mechanically flexible tunneling contact

A. Isacsson
Department of Applied Physics, Chalmers University of Technology and Göteborg University, S-412 96 Göteborg, Sweden
(Received 22 December 2000; revised manuscript received 2 April 2001; published 29 June 2001)

The dynamics of a nanoelectromechanical system in the form of a mechanically deformable three-terminal metallic tunneling device is studied by analytical and numerical methods in the absence of single charging effects. The coupling of electronic charge transport to the mechanical degree of freedom leads to a dynamical instability characterized by limit-cycle behavior. Furthermore, the existence of two stable stationary points may lead to directly detectable deterministic chaotic motion.

DOI: 10.1103/PhysRevB.64.035326 PACS number(s): 73.40.Gk, 77.65.Fs, 07.10.Cm

I. INTRODUCTION

The growing interest in nanoelectromechanical systems (NEMS) is partly due to the advances in microfabrication by self-assembly of biometallic composites where metallic or semiconducting clusters are combined with organic molecules such as polymers or DNA.[1–5] Since the organic chain molecules used in self-assembly are typically a few orders of magnitude softer[6–8] than ordinary solids, their utilization in nanoelectronics implies that mechanical degrees of freedom can have great impact on the electronic transport properties in such systems.

We have previously[9,10] investigated how the mechanical degrees of freedom couple to the electrical transport properties in a Coulomb blockade double junction where the central island is free to move in a parabolic potential. A dynamical instability was shown to exist in this structure that caused the central island to oscillate between the external electrodes. In the low-temperature limit, where charging effects are important, this instability gave rise to a mechanically mediated current that approached the value $I=2eNf$ where e is the elementary charge, N the maximum number of excess electrons allowed on the island, and f the frequency of elastic vibrations. The fluctuations of this current have been shown to disappear exponentially with decreasing temperatures,[11] implying that this system may be well suited for current standard purposes. In realizing a current standard device of this type, a grain placed on a flexible cantilever positioned between the two electrodes can replace the grain and the soft molecular links considered in Refs. 9,10. Such nanoscale mechanical resonators have successfully been fabricated.[12,13] It has also been suggested by Tuominen *et al.*,[14] who studied a macroscopic electromechanical system at room temperature, that carbon nanotubes connected to nanoscale metallic grains,[15,16] could be used for this purpose.

In this paper, it is shown that when a system consisting of a grain attached to the tip of a cantilever by a tunnel junction [see Fig. 1(a)] is treated as a three-terminal device it shows a rich dynamical structure ranging from stable limit-cycle behavior to deterministic chaos. Since this paper focuses on the dynamical properties, the temperature is considered to be large enough for charging effects to be absent, while still low enough for thermal fluctuations to be negligible.

The same model also applies to the dynamics of the single-electron transistor structure in Fig. 1(b). The central island is here resting on a mechanically soft insulating monolayer allowing for center-of-mass motion of the grain. This system should of course be studied in the low-temperature limit where charging effects are of importance. However, since much of the dynamical features of the system in the high-temperature limit are expected to survive at lower temperatures, the results obtained in this paper are of interest for further studies in the low-temperature regime.

II. MODEL SYSTEM

The system, as depicted in Fig. 1(a) consists of a small metallic grain, typically a few nanometers in diameter, attached to the tip of a metallic cantilever through a tunnel

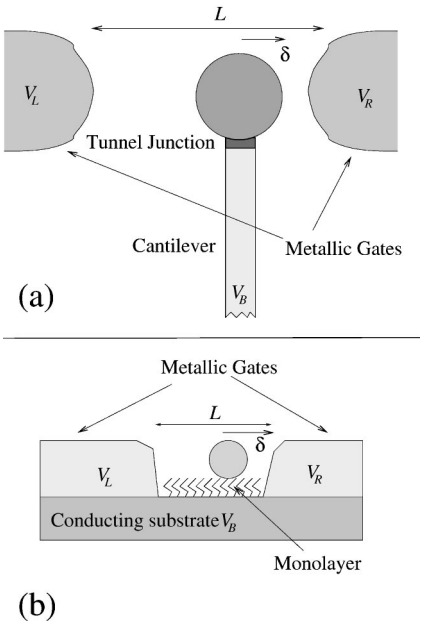

FIG. 1. Schematic layout of the system. (a) A cantilever attached to a conducting grain through a tunnel junction situated asymmetrically between two metallic electrodes separated by a distance L. The electrodes and the cantilever are biased with voltages V_L, V_R, and V_B, respectively. The distance between the grain and the electrodes are such that electrons may tunnel through the structure. (b) Self-assembled single-electron transistor structure. The dynamical features discussed for system (a) are relevant also for this system.

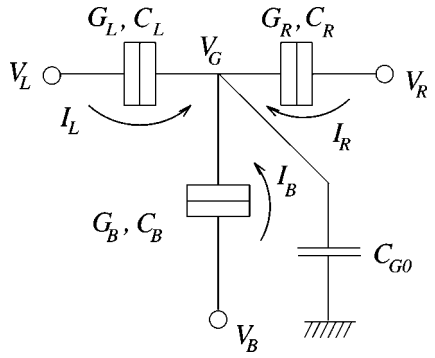

FIG. 2. Electric circuit model. Each tunnel junction is modeled by a capacitor in parallel with a tunnel resistance $R_{L,R,B}=G_{L,R,B}^{-1}$. Furthermore, the grain-ground capacitance has been taken into account through the capacitance C_{G0}. Only the ''nearest neighbor'' capacitances are considered in this model.

junction. The other end of the cantilever is assumed to be clamped and connected to a voltage source V_B. The grain attached to the cantilever is situated between two metallic electrodes located close enough to the grain to allow tunneling but with tunneling resistances much larger than that of the grain-cantilever junction. If the typical frequency of the dynamical motion of the system is well below the plasma frequency of the metallic components, the charges and potentials on the conductors are related by the matrix C_{ij};[17]

$$Q_i=\sum_j C_{ij}V_j.$$

The system can then be mapped onto an electrical network model seen in Fig. 2. In this model, only ''nearest neighbor'' coefficients in C_{ij} have been taken into account. Each tunnel junction is modeled by a resistance R in parallel with a capacitance C, the latter being related to the coefficients C_{ij} by linear transformations. Using this model, the grain-potential V_G can be expressed in terms of the grain-charge Q_G and the applied bias voltages $V_{R,L,B}$ (cf. Fig. 1) as

$$V_G(Q_G)=\frac{Q_G+V_RC_R+V_LC_L+V_BC_B}{C_\Sigma},$$

where $C_\Sigma=C_L+C_R+C_B+C_{G0}$. The currents $I_{L,R,B}$ flowing from the electrodes to the grain, as shown in Fig. 2, determine an equation of motion for Q_G;

$$\frac{dQ_G}{dt}=I_L+I_R+I_B.$$

Using $I_{L,R,B}=(V_{L,R,B}-V_G)G_{L,R,B}$, where $G_{L,R,B}$ are conductances of the tunnel junctions (cf. Fig. 2) one finds

$$\frac{dQ_G}{dt}=V_LG_L+V_RG_R+V_BG_B-V_G(G_L+G_R+G_B).$$

The flexibility of the cantilever allows for a mechanical degree of freedom in the system. We will assume that this freedom is one dimensional, i.e., that the cantilever only bends in one direction and that this bending is so small that we can consider the grain to move on a straight line between the two electrodes. The deflection δ of the grain from the equilibrium position towards the right electrode is described by the equation of motion

$$\ddot{\delta}+\gamma\dot{\delta}+\omega_0^2\delta=\mathcal{E}Q_G/m,$$

where ω_0 is the elastic frequency of the system and γ a phenomenological parameter introduced to account for dissipation of mechanical energy. Although the use of Stokes friction is valid for the cantilever setup in Fig. 1(a) it may not be appropriate for the type of setup of Fig. 1(b) where the precise mechanism of dissipation is more unclear. The mass m appearing on the right-hand side is an effective mass depending on the precise geometry and design of the cantilever-grain system. In the force term only the effect of the electrostatic field between the left and right electrodes $\mathcal{E}\approx(V_L-V_R)/L$ to linear order in Q_G has been considered. For this approximation to be valid, and for the island not to get stuck close to one electrode, it is important that the minimum grain-lead separation is large enough for adhesive forces (mainly cohesion[18] and van der Waals interaction[19]) to be negligible compared to the electrostatic force.

The tunneling conductances $G_{L,R}$ have a sensitive dependence on the grain displacement δ

$$G_{L,R}=G_{L,R}^0\exp\left(\mp\frac{\delta}{\lambda}\right),$$

where the tunneling length λ is determined by the work function ϕ of the electrodes,

$$\lambda\approx\left(\frac{2\sqrt{2m_e\phi}}{\hbar}\right)^{-1}.$$

The variations of the capacitances with position have been neglected since they are much smaller than the changes in the conductances that dominate the nonlinear behavior of the system. By measuring the deflection δ in units of lambda i.e., $\delta=\xi\lambda$, one arrives at the following system of equations,

$$\dot{\xi}=\Pi, \tag{1}$$

$$\dot{\Pi}=-\gamma\Pi-\omega_0^2\xi+\left(\frac{V_L-V_R}{Lm\lambda}\right)Q_G, \tag{2}$$

$$\dot{Q}_G=V_LG_L^0e^{-\xi}+V_RG_R^0e^{\xi}+V_BG_B-V_G(Q_G)G_\Sigma, \tag{3}$$

where

$$G_\Sigma(\xi)=G_L^0e^{-\xi}+G_R^0e^{\xi}+G_B, \tag{4}$$

and

$$V_G(Q_G)=\frac{Q_G+V_LC_L+V_RC_R+V_BC_B}{C_\Sigma}. \tag{5}$$

III. FIXED POINTS AND STABILITY

In order to characterize the dynamical behavior of the system, the existence of fixed points is investigated and then

the stability of these points is considered. Throughout the rest of the paper the right electrode potential will be used as reference, i.e., we will put $V_R=0$ from here on. With this convention, the stationary points satisfy the following system of equations:

$$\begin{cases} 0 &= \Pi \\ 0 &= -\gamma\Pi-\omega_0^2\xi+\left(\dfrac{V_L}{Lm\lambda}\right)Q_G \\ 0 &= V_L G_L^0 e^{-\xi}+V_B G_B-\dfrac{Q_G+V_L C_L+V_B C_B}{C_\Sigma}G_\Sigma(\xi). \end{cases} \tag{6}$$

Defining $\alpha\equiv\omega_0^2 Lm\lambda/C_\Sigma$, $\eta^2=V_L^2$ and $\sigma=V_L V_B$, Eq. (6) can be recast in the form $\alpha\xi=H(\xi)$ where

$$H(\xi)=\frac{\eta^2 g_L e^{-\xi}+\sigma}{g_L e^{-\xi}+g_R e^{\xi}+1}-(\eta^2 c_L+\sigma c_B).$$

Here, the dimensionless conductances $g_{R,L}=G_{R,L}^0/G_B$ and capacitances $c_{L,B}=C_{L,B}/C_\Sigma$ have been introduced. Since $H(\xi)$ is a restricted function, the equation $\alpha\xi=H(\xi)$ has at least one solution, and at the most, three solutions. Defining $\vartheta=\eta^2/\sigma=V_L/V_B$, three different cases can be identified,

- $\vartheta<0$, $H(\xi)$ has one minimum located at $\xi_0=\frac{1}{2}\ln([1-\vartheta]g_L/g_R)$ which means that the system has either one or three fixed points.
- $0<\vartheta<1$, $H(\xi)$ has one maximum located at $\xi_0=\frac{1}{2}\ln([1-\vartheta]g_L/g_R)$ and again we may have either one or three fixed points.
- $\vartheta>1$, In this case $H(\xi)$ is monotonic hence only one fixed point can exist.

When $\vartheta<0$ two different cases can be distinguished; $\vartheta<-c_B/c_L$ and $0>\vartheta>-c_B/c_L$. In the first case, $\lim_{\xi\to+\infty}H(\xi)<0$ and only one solution lying in the left half plane is possible. In the second case, the corresponding limit is positive and if α is chosen small enough, three solutions will appear, one in the left half plane and two in the right. The different scenarios are shown in Fig. 3. When $0<\vartheta<1$, one can again single out two cases; $c_B/(1-c_L)<\vartheta<1$ and $0<\vartheta<c_B/(1-c_L)$. When $c_B/(1-c_L)<\vartheta<1$, then $\lim_{\xi\to-\infty}H(\xi)>0$ and only one solution located in the right half plane is possible. In the other case, the limit is negative and one can find two more solutions in the left half plane by choosing α sufficiently small.

A stability analysis of the fixed points, obtained above shows that: In the case of only one fixed point, this point will be a stable node, i.e., all eigenvalues Jacobian of the system are real and negative,[20] if the damping γ exceeds the critical damping γ_c,

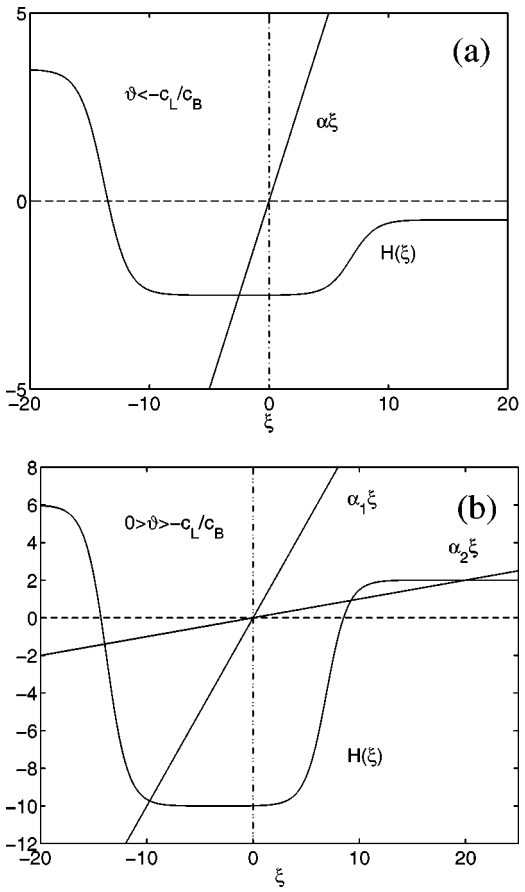

FIG. 3. Solutions to the fixed-point equation $\alpha\xi=H(\xi)$. When $\vartheta=V_L/V_B<0$, either one or three solutions exist depending on whether ϑ is larger or smaller than the ratio $-C_L/C_B$ and what value $\alpha\propto\omega_0^2$ assumes. In (a), only one stationary point exists while in (b), either one or three stationary points appear.

$$\gamma_c=-\frac{1}{2}\left[\tau^{-1}(\xi)+\omega_0^2\tau(\xi)-\sqrt{[\tau^{-1}(\xi)+\omega_0^2\tau(\xi)]^2-4\frac{\omega_0^2 H'(\xi)}{\alpha}}\right]. \tag{7}$$

Here, the total RC-time $\tau(\xi)$ is defined as

$$\tau^{-1}(\xi)\equiv\frac{G_\Sigma(\xi)}{C_\Sigma}=-\frac{\partial\dot{Q}_G}{\partial Q_G}.$$

In the case of three fixed points, one will be conditionally stable depending on whether γ is larger or smaller than γ_c. The second ''middle'' one [cf. Fig. 3(b)] will not be a node but instead, will be a saddle point of index one (two negative and one positive eigenvalue of the Jacobian), and hence, not a stationary point irrespective of the value of γ, while the remaining point [corresponding to the rightmost solution in Fig. 3(b)] will always be a stable node.

IV. STATIONARY OPERATION

When $\sqrt{\alpha}$, which is proportional to the frequency of elastic vibrations ω_0, is large compared to the applied bias volt-

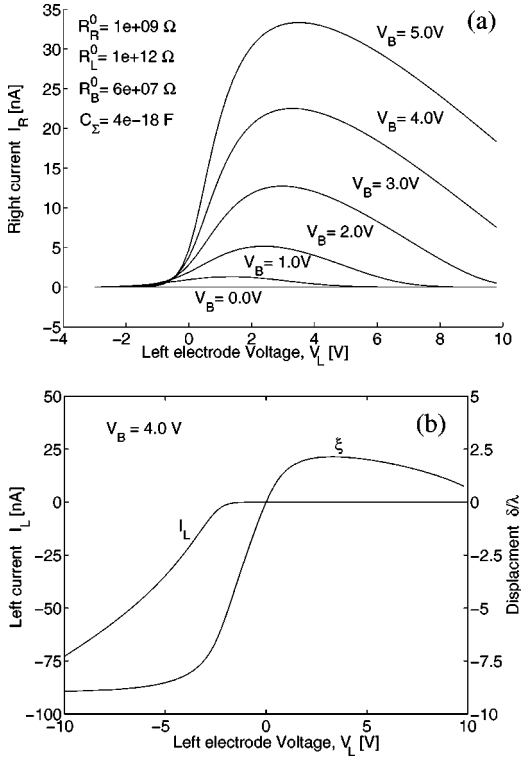

FIG. 4. Stationary operation. When the damping constant γ is large, the static deflection of the cantilever will cause a pronounced transistorlike action due to the exponential decrease of the tunneling resistance between the grain and the right electrode (a) Current flowing from the grain to the right electrode as a function of the voltage V_L applied to the left electrode. The different curves correspond to different biases V_B applied to the bottom electrode. In (b), the displacement δ of the cantilever and the current flowing from the left electrode to the grain is plotted for the case $V_B=4.0$ V.

ages, one expects to find only one stationary solution as discussed above. In Fig. 4(a) the $I-V$ characteristics for this case is shown for an asymmetric setup with $R_R^0=1$ GΩ, $R_L^0=1$ TΩ, $R_B=6$ MΩ and all capacitances set to 1 aF. The frequency of elastic vibrations was set to 4.4 GHz. The figure shows the current flowing from the grain to the right electrode (as opposed to I_R, defined in Fig. 2, which was defined in the opposite direction) as a function of the voltage applied to the left electrode. The different curves correspond to different biases applied to the bottom electrode. For negative V_L, almost no current flows in the system, since the grain is essentially disconnected from both leads. As the field is increased, the cantilever will start to deflect towards the right electrode, causing an exponential decrease in R_L allowing the current to grow.

As V_L is further increased, the charge on the grain will eventually become negative due to the capacitive coupling to the left electrode resulting in a decreased deflection disconnecting it from the leads once again. In Fig. 4, the displacement of the grain along with the current flowing to it from the left electrode, is shown as a function of V_L when $V_B=4.0$ V. This current is essentially zero until a bias of approximately -3.0 V is reached. Furthermore, from this graph it can be seen that the displacement of the grain is just

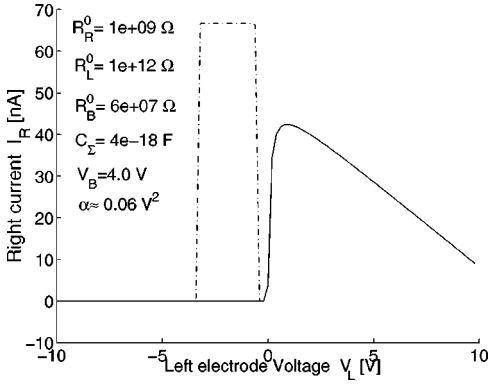

FIG. 5. Bistable operation. When α is small enough, two stable fixed points emerge leading to a bistable situation. The solid line corresponds to the ''expected'' solution, while the dashed lines correspond to the new second stable root to the fixed-point equations.

a few times λ (for Au λ is typically 0.5 Å).

For $\sqrt{\alpha}$ small compared to the applied bias voltages, it is possible to have two stable fixed points in the system. Using exactly the same parameters as above, but with a reduced α, this second solution appears. In Fig. 5, the $I-V$ characteristics of this *bistable mode* is shown. The solid line correspond to the same solution as above and the dashed solution to the new one that appears due to the reduced α.

V. DYNAMICAL OPERATION

In the dynamical regime, the system displays a rich structure. One of the most interesting features is that this is a nanoscale system with directly detectable chaotic behavior. This means that in order to determine what type of motion the system exhibits, it is sufficient to monitor the currents. Due to the multitude of parameters and the system's complex dependence on these, only a few archetypical cases will be illustrated by means of numerical integration of the equations of motion (1)–(5). In the presented simulations, a system with the same parameters as in the static case (see the previous section) is considered but with a damping rate γ reduced below γ_c. The different simulations then correspond to different sets of bias voltages V_B and V_L.

A. One Fixed Point

We first consider the situation when the system has only one fixed point corresponding to the situation in Fig. 3(a). This is achieved by using a fixed voltage $V_B=3$ V and imposing a positive bias voltage V_L. For small values of this voltage the system remains stable, as expected, until a critical threshold voltage is reached. Further biasing leads, for positive V_L, to a limit-cycle regime. For the range of positive voltages where the algorithm was stable, this cycle remained. For negative bias voltages, there exists a threshold voltage as well, and as this is reached, a stable limit cycle appears. An example of this type of motion is shown in Fig. 6 (recorded at $V_L=-0.35$ V). Decreasing V_L moves the system toward the situation in Fig. 3(b), i.e., we approach the

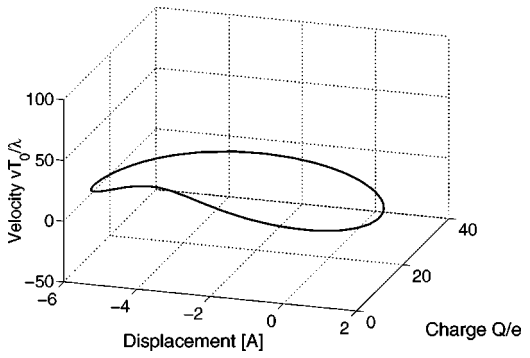

FIG. 6. Phase-space trajectory for a stable limit cycle. As the damping γ is reduced below the critical damping γ_c the system settles in to a stable limit cycle.

situation with three fixed points. This leads to a sequence of period doublings. The behavior in this regime is illustrated in Fig. 7(a). These period doublings can be directly detected by simultaneously measuring the currents I_B and I_L and plotting them as in Fig. 7(b). Lowering the bias more eventually leads to a totally chaotic regime like the one in Fig. 8 ($V_L = -0.6$ V) which is again reflected in the currents. Further lowering of V_L after this point leads to an alternating series of period-doubled limit cycles and chaotic trajectories until three fixed points appear in the system.

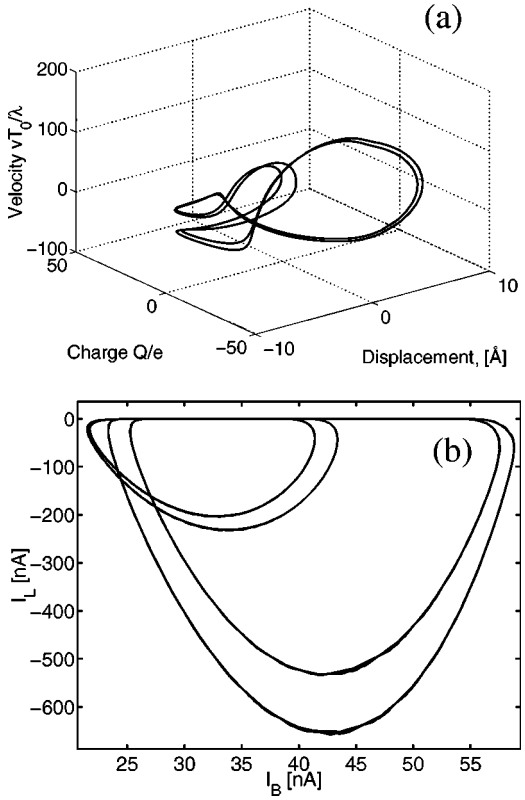

FIG. 7. Multiply period-doubled phase-space trajectory and the corresponding plot of the currents I_L and I_B. (a) Biasing the system towards the situation with three fixed points will cause subsequent period doublings of the limit cycle. (b) By monitoring the currents flowing in the left lead and the bottom lead at the same time these period doublings can be detected.

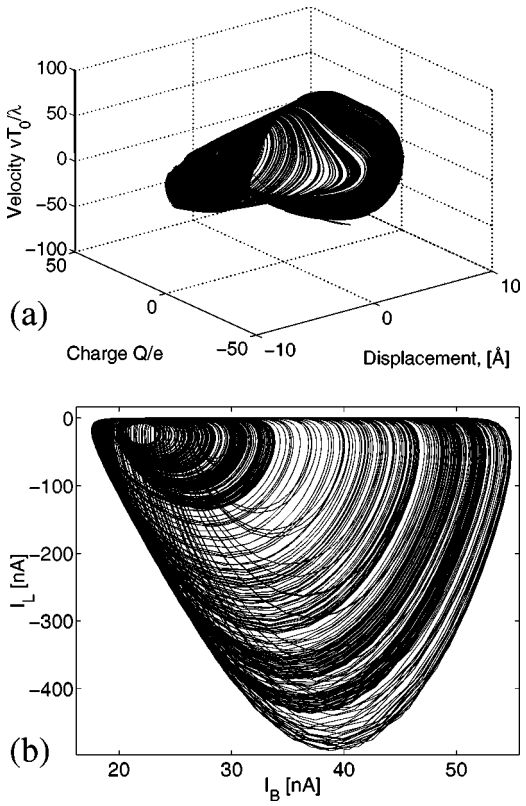

FIG. 8. Chaotic motion. (a) Phase-space trajectory in the chaotic regime. Biasing the system very close to the situation with three fixed points the system becomes chaotic. (b) Chaos is also reflected in the corresponding plot of the currents I_L and I_B.

B. Three Fixed Points

In order to be able to study the case with three fixed points, V_B was raised to 6 V while V_L was set to 0.7 V. This corresponds to the situation with three solutions in Fig. 3(b). Numerical integration revealed the structure displayed in Fig. 9. Starting close to the conditionally stable fixed point, the leftmost one in Fig. 3(b), a stable limit cycle is eventually

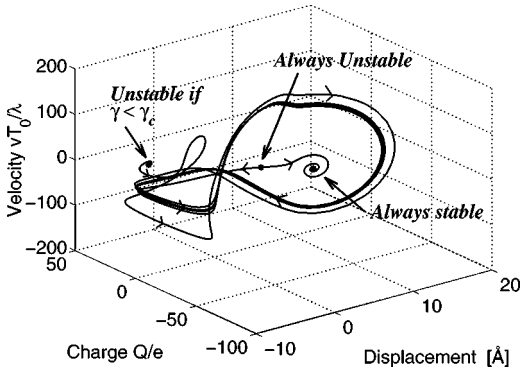

FIG. 9. Phase-space trajectory when three fixed points are present. When the system has three fixed points, one of them will always be stable, one will always be unstable, and one will be unstable if $\gamma < \gamma_c$. The three fixed points are indicated by * in the figure. The stable limit cycle that exists in this case can also be seen in the figure.

reached. Starting the simulation in the vicinity of the middle one (always unstable) the trajectory either connects to this limit cycle or becomes attracted by the third fixed point, which is always stable.

VI. CONCLUSIONS

We have shown that the three-terminal flexible tunneling structures in Fig. 1, which are of interest for both current standard purposes, as well as for self-assembled quantum devices, have several characteristic dynamical features: When the damping γ in the system is high (low-quality factor) the system displays a stationary behavior, which for some parameter values, can be bistable. If the quality factor is large enough, i.e., the damping satisfies $\gamma < \gamma_c$, the dynamics of the system range from stable limit-cycle behavior to deterministic chaos. It is furthermore possible to have a situation where stable fixed points coexist with stable limit cycles. The chaotic motion of the system can be directly detected by measuring the currents flowing from the terminals.

ACKNOWLEDGMENTS

The author would like to acknowledge Leonid Gorelik, Robert Shekhter, and Sara Blom for fruitful discussions. This work has been supported by the Swedish Research Council for Engineering Sciences (TFR) and the Swedish Strategic Research Foundation (SSF) program ''Quantum Devices and Nano-Science.''

[1] R.P. Andres, J.D. Bielefeld, J.I. Henderson, D.B. Janes, V.R. Kolagunta, C.P. Kubiak, W.J. Mahoney, and R.G. Osifchin, Science **273**, 1690 (1996).
[2] E. Braun, Y. Eichen, U. Sivan, and G. Ben-Yoseph, Nature (London) **391**, 775 (1998).
[3] R. Elghanian, J.J. Storhoff, R.C. Mucic, R.L. Letsinger, and C.A. Mirkin, Science **277**, 1078 (1997).
[4] C.A. Mirkin, R.L. Letsinger, R.C. Mucic, and J.J. Storhoff, Nature (London) **382**, 607 (1996).
[5] A.P. Alivastos, K.P. Johnsson, X. Peng, T.E. Wilson, C.J. Loweth, M.P. Bruchez Jr, and P.G. Schultz, Nature (London) **382**, 609 (1996).
[6] O. Alvarez and R. Latorre, Biophys. J. **21**, 1 (1978).
[7] S.B. Smith, Y. Cui, and C. Bustamente, Science **271**, 795 (1996).
[8] S.B. Smith, L. Finzi, and C. Bustamente, Science **258**, 1122 (1992).
[9] L.Y. Gorelik, A. Isacsson, M.V. Voinova, B. Kasemo, R.I. Shekhter, and M. Jonson, Phys. Rev. Lett. **80**, 4526 (1998).
[10] A. Isacsson, L.Y. Gorelik, M.V. Voinova, B. Kasemo, R.I. Shekhter, and M. Jonson, Physica B **255**, 150 (1998).
[11] C. Weiss and W. Zwerger, Europhys. Lett. **47**, 97 (1999).
[12] A. Erbe, R.H. Blick, A. Tilke, A. Kriele, and J.P. Kotthaus, Appl. Phys. Lett. **73**, 3751 (1998).
[13] A. Erbe, C. Weiss, W. Zwerger, and R.H. Blick, cond-mat/0011429 (unpublished).
[14] M.T. Touminen, R.V. Krotkov, and M.L. Breuer, Phys. Rev. Lett. **83**, 3025 (1999).
[15] J. Liu, A.G. Rinzler, H. Dai, J.H. Hafner, R.K. Bradley, P.J. Boul, A. Lu, T. Iverson, and K. Shelimov, Science **280**, 1253 (1998).
[16] P. Poncharal, Z.L. Wang, D. Ugarte, and W.A. de Heer, Science **283**, 1513 (1999).
[17] D.K. Ferry and S.M. Goodnick, *Transport in Nanostructures* (Cambridge University Press, Cambridge, England, 1997), Chap. 4.
[18] C.J. Cheng, J. Phys.: Condens. Matter **3**, 1227 (1991).
[19] J. N. Israelachvili, *Intermolecular and Surface Forces* (Academic Press, London, 1985), Chap 11.
[20] R.C. Hilborn, *Chaos and Nonlinear Dynamics* (Oxford University Press, New York, 1994), Chap. 4.